# Analysis of the Capacitor-Less D-STATCOM for Voltage Profile Improvement in Distribution Network With High PV Penetration

Rohouma, Wesam; Metry, Morcos; Balog, Robert S.; Peerzada, Aaqib Ahmad; Begovic, Miroslav M.; Zhou, Dao

*Published in:*
IEEE Open Journal of Power Electronics

*DOI (link to publication from Publisher):*
10.1109/OJPEL.2022.3167548

*Publication date:*
2022

# Analysis of the Capacitor-less D-STATCOM for Voltage Profile Improvement in Distribution Network with High PV Penetration

Wesam Rohouma, *Member, IEEE, Morcos Metry, Member, IEEE,* Robert S. Balog, *Senior Member, IEEE,* Aaqib Ahmad Peerzada, *Student Member, IEEE*, Miroslav M. Begovic, *Fellow, IEEE, Dao Zhou, Senior Member, IEEE*

**Abstract-** Distributed Energy Resources (DERs) have disrupted the traditional electrical system. Grid-connected photovoltaic (PV) systems deliver electric energy closer to the consumer, shifting the paradigm from centralized to distributed generation. However, the impact of the stochastic PV output power gives rise to potentially rapid voltage fluctuations. Reactive power compensation is needed to regulate the voltage profile to meet the relevant standards. However, switched capacitors, a traditional approach, cannot provide reactive power that is continuously-adjustable at short time scales of minutes or seconds. Recently, smart inverters have been tasked to provide ancillary services including reactive power support; the impact on the reliability, operational constraints, and cost to the inverter are actively being studied. This paper examines an alternative, a distribution static synchronous compensator (D-STATCOM) based on a matrix converter (MC) for use in the low voltage distribution network. This technology is capable of long service life because it uses inductors for energy storage instead of electrolytic capacitors. The contribution of this paper is a detailed analysis and impact study of the capacitor-less D-STATCOM in high PV penetration distribution networks. The significance of this paper is that it studies the behavior of the power electronics converter and its interaction with the power systems, without assuming or neglecting details of either.

***Index Terms*— D-STATCOM, Voltage profile, Reactive power compensation, Model predictive control, Matrix converter, Grid integration of renewable energy sources.**

## NOMENCLATURE[1]

| | |
|---|---|
| $T_S$ | Sampling time |
| $k$ | Discrete sample time step |
| $\sigma$ | Switching configuration number, $\sigma \in \{1,..,27\}$ |
| $j$ | Phase $j \in \{A, B, C\}$ |
| $V_{oj}$ | Per-phase output voltage of the matrix converter |
| $I_{oj}$ | Per-phase output current of the matrix converter |
| $L_{MCj}$ | Per-phase output inductors |
| $R_{L_{MCj}}$ | Per-phase parasitic resistance on output inductors |
| $V_{Busj}$ | Per-phase input voltage of the filter |
| $V_{ej}$ | Per-phase input filter output voltage (matrix converter input voltage) |
| $\dot{V_{ej}}$ | Per-phase first order derivative of the input filter output voltage (matrix converter input voltage) |
| $I_{cj}$ | Per-phase input filter output current (matrix converter input current) |
| $\dot{I_{cj}}$ | Per-phase first order derivative of the input filter output current (matrix converter input current) |
| $I_{ej}$ | Per-phase output current of the filter |
| $R_{fj}$ | Per-phase parasitic resistance of the filter inductors |
| $L_{fj}$ | Per-phase filter inductors |
| $C_{fj}$ | Per-phase filter capacitors |
| $i_{cj}^*$ | Reference input current in the MPC cost function |
| $i_{oj}^*$ | Reference output current in the MPC cost function |
| $\lambda_1, \lambda_2$ | MPC cost function weighting factors |
| $F_{sw}$ | Matrix converter switching frequency |
| $I_{Lj}$ | Per-phase load current |
| $S_{ij}(t)$ | The switching function for $i$ is an element of {A,B,C} and $j$ is an element of {a, b, c} $S \in \{0,1\}$ |
| $Z_n$ | Feeder impedance on the low voltage distribution network between bus-1 and bus-2 $(R_n + jX_n)$ |
| $\Delta V_g$ | Voltage deviation between bus-1 and bus-2 |
| $\alpha, \beta$ | Parameters that define the exponential relationship of voltage with load active and reactive power |
| $\psi_j^p$ | The rated peak active power of j$^{th}$ PV system |
| $P_i^p$ | Peak active load injection at $i^{th}$ bus |
| $r$ | Total number of PV systems deployed |
| $N$ | Total number of buses in the distribution system |
| $Q_{cb}$ | The reactive power exchanged between the converter and the bus where the converter is connected |

[1]This publication was made possible by NPRP grant # 9-204-2-103 from the Qatar National Research Fund (a member of Qatar Foundation). The statements made herein are solely the responsibility of the authors. The authors acknowledge Prof. Pat Wheeler and Prof. Lee Empringham.

Wesam Rohouma is with the College of the North Atlantic University in Qatar (email: wesam.rohouma@ieee.org)

Morcos Metry and Robert S. Balog are with the Renewable Energy & Advanced Power Electronics Research Laboratory, Department of Electrical & Computer Engineering, Texas A&M University at Qatar, Doha, QATAR (e-mails: morcos.m.metry@ieee.org, robert.balog@ieee.org).

Aaqib Ahmad Peerzada and Miroslav M. Begovic are with the Department of Electrical & Computer Engineering, Texas A&M University, College Station, TX, USA (e-mails: peerzada@tamu.edu, begovic@tamu.edu).

Dao Zhou is with the Department of Energy Technology, Aalborg University, 9220 Aalborg, Denmark, (email: zda@et.aau.dk).

| | |
|---|---|
| $B, G$ | Line susceptance and the conductance respectively |
| $V_{pcc}$ | Voltage at the point of common coupling |
| $V_{conv}$ | Converter voltage |
| $F_{conv}(t)$ | Failure cumulative distribution function of a converter over time $t$ in years |
| $F_{com}(t)$ | Failure cumulative distribution function of a component |
| $\lambda_Q, \lambda_D$ | Failure rate per year for the switch and diode respectively |
| $\lambda_E$ | Failure rate of energy storage device $\lambda_C$ for capacitors and $\lambda_L$ for inductors |
| $n_E\ n_Q n_D$ | Number of components (energy devices, switches, and diodes respectively) in converter topology |
| $B_{10}$ | The time (years) by which the converter has 10% probability of failure |

# I. Introduction

# II. The Big Picture Impact of The Capacitorless D-STATCOM on Power Quality Improvement

Consider the big picture system one-line diagram of an example distribution system in Fig. 1. In addition to increasingly residential and commercial penetration of non-linear loads and renewable energy, this illustrative example considers a bus system with high utility-scale PV penetration. The impact of the capacitorless D-STATCOM voltage regulation is studied in this paper.

## *A. Technical challenges of increased penetration of PV systems in the distribution network*

As the penetration levels of PV systems in distribution network increase, a range of adverse power quality problems [50, 51] may appear including:

- Reverse power flow: the increased proliferation of PV systems may offset local feeder loads and lead to reverse power flow that may affect overcurrent protection devices and operation of voltage regulating equipment.
- Voltage rise: the voltage rise can be significant when large PVs are connected at the end of lightly loaded feeders. Voltage violation may happen and can trigger the overvoltage protection equipment.
- Voltage fluctuations: shading and cloud cover of PV systems can cause variations in output power, and this can have a significant impact on feeder voltage.
- Interaction with available voltage regulating equipment: voltage rise and fluctuations may lead to the increased switching operation of voltage-controlled CBs, OLTC and line voltage regulators.
- Changes in feeder loading and electric losses: large penetration may lead to reverse power flow that may lead to increased power losses. Also, voltage rise may also lead to an increase in customer energy consumption (opposite to conservative voltage reduction method).

Voltage rise, voltage fluctuations, current and voltage harmonics are among the prominent problems in distribution feeders. The severity of these problems depends on PV penetration level, location of the PV, voltage control equipment such as voltage regulators and capacitor banks in distribution feeder. These problems have a direct impact on network equipment. Voltage variations cause frequent operation of OLTC, line voltage regulators (VRs) and voltage-controlled capacitor banks for controlling the feeder voltage. This frequent operation shortens the expected life cycle of these devices and increases maintenance requirements [52, 53].

## *B. The role of capacitorless D-STATCOM in distribution networks*

A distribution static synchronous compensator (D-STATCOM) is a fast response power electronics device that can provide flexible voltage regulation, power factor correction, and harmonics mitigation in the distribution network [18, 25-36]. In electrical distribution systems, the motivations for providing reactive power support include minimization of feeder losses, flattening of feeder voltage profile and improvement of substation power factor. In some cases, the dynamic dispatch of local volt-ampere reactive (VAR) compensation can also help in extending the low-voltage ride-through capability of the system, thereby mitigating the possibility of short-term voltage collapse. The reactive power support, one that can be continuously adjusted will help reduce the operational stress on the slow-acting mechanically switched devices, such as step-type voltage regulators and switchable capacitor banks. Such a reactive power support source could either be run autonomously to achieve a set of predefined objectives or can be dispatched by the system operator.

In case the system operator wants to improve the power factor at a particular bus, the dispatch command will trigger the compensator to measure and supply the local reactive demand at the point of common coupling. Whereas, if the objective is to reduce the frequency of operation of the electromechanical devices on the feeder, the dispatch command could take the form of voltage regulation, at the bus injection location. In the first scenario, the power quality compensator is expected to supply the local reactive power demand, thus eliminating the need of supplying the reactive power from the source/substation. In the second scenario, the power quality compensator is expected to autonomously determine the required VARs to be produced or consumed, to maintain the voltage within some determined limits. The current mechanical assets for voltage control operate on a slower time scale as compared with the intermittency associated with the solar PV power injections. This mismatch renders the mechanically switched devices inadequate to correct the fast voltage variations.

# III. Control Strategy of the Capacitorless D-STATCOM System

In terms of impact and behavior the capacitorless D-STATCOM is designed to perform the same functions as the incumbent voltage source converter-based (VSC) D-STATCOM technology. The only difference between the proposed capacitorless D-STATCOM and the incumbent D-STATCOM is the use of inductors instead of capacitors for energy storage. This section explains the control strategy that allows a matrix converter to rely on inductive energy storage

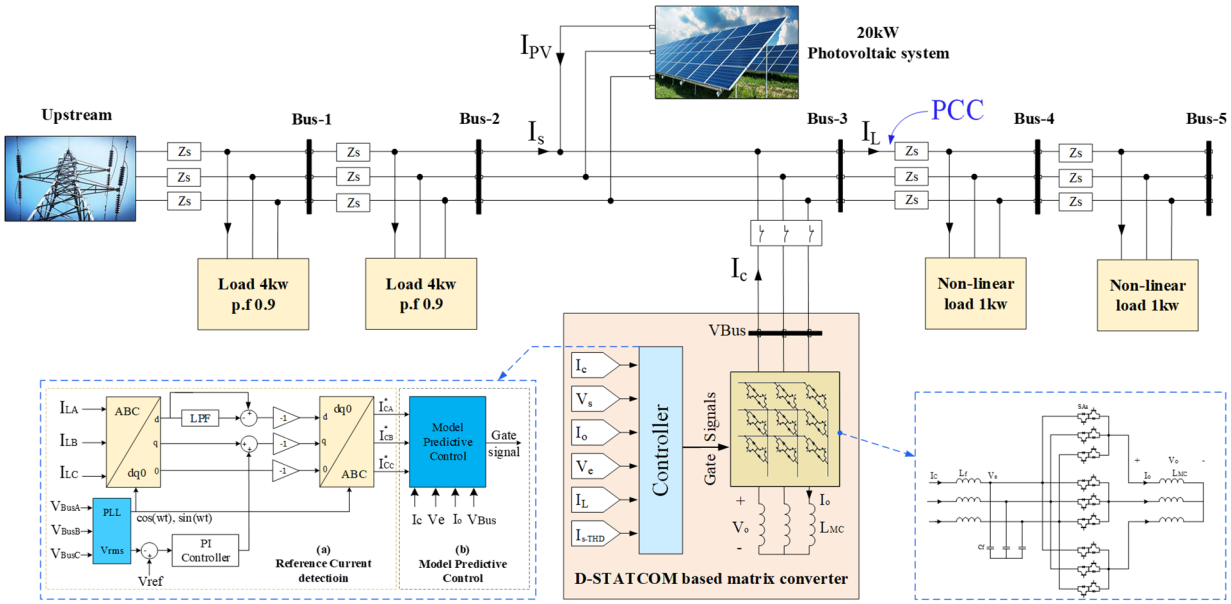


Fig. 2 Detailed example system showing the capacitorless D-STATCOM device shunt connected at bus-3 Other buses in the vicinity are labeled as shown. Without loss of generality, the remainder of the distribution system to the sub-station is shows as "upstream."

perform as a capacitorless D-STATCOM.

### *A. Topology of the matrix converter*

Consider the detailed system, showing the capacitor-less D-STATCOM based matrix converter topology, as shown in Fig. 2. The capacitorless D-STATCOM consists of a three-phase matrix converter (MC) system connected to the PCC through an input filter and the MC output is connected to an inductive energy storage element $L_{MC}$. The proposed D-STATCOM is controlled using finite control set model predictive control (FCS-MPC).

The matrix converter is a type of power electronics converters that can perform direct ac/ac power conversion without the use of electrolytic dc capacitors, and this will increase its reliability and service life in comparison to the traditional VSC [54]. As shown in Fig. 2, the power circuit of the matrix converter consists of nine bidirectional switches each comprised of two IGBT and diode pairs connected in anti-parallel to support bidirectional current flow. The MC is connected to the distribution network through an input filter to prevent the high frequency switching harmonics from propagating to the network.

### *B. The role of current reversal for inductive storage*

The MC is appropriately controlled by MPC to enable the input to output current phase inversion. By using the property of current phase reversal, the converter absorbs leading currents from the ac network while the inductor absorbs lagging current at the output side of the converter.

The output voltages and input currents of the MC were calculated according to (1), (2) and (3) as a function of MC input voltages, output currents and the switching function. The inductive load constrains the switching to avoid interruption of MC output current. The voltage-source input constrains the switching to avoid shorting the input phases. This constraint can be expressed as:

$$\begin{bmatrix} V_{oA} \\ V_{oB} \\ V_{oC} \end{bmatrix} = \begin{bmatrix} S_{Aa} & S_{Ab} & S_{Ac} \\ S_{Ba} & S_{Bb} & S_{Bc} \\ S_{Ca} & S_{Cb} & S_{Cc} \end{bmatrix} . \begin{bmatrix} V_{eA} \\ V_{eB} \\ V_{eC} \end{bmatrix} \quad (1)$$

$$\begin{bmatrix} I_{cA} \\ I_{cB} \\ I_{cC} \end{bmatrix} = \underbrace{\begin{bmatrix} S_{Aa} & S_{Ab} & S_{Ac} \\ S_{Ba} & S_{Bb} & S_{Bc} \\ S_{Ca} & S_{Cb} & S_{Cc} \end{bmatrix}}_{M} . \begin{bmatrix} I_{oA} \\ I_{oB} \\ I_{oC} \end{bmatrix} \quad (2)$$

$$S_{Aj} + S_{Bj} + S_{Cj} = 1 \quad \forall \quad j \in \{A, B, C\} \quad (3)$$

where $M$ is the instantaneous transfer matrix, $V_{oA}(t)$, $V_{oB}(t)$, $V_{oC}(t)$ and, $I_{oA}(t)$ $I_{oB}(t)$, $I_{oC}(t)$ are the output voltages and currents of the matrix converter, respectively. While, $V_{eA}(t)$, $V_{eB}(t)$, $V_{eC}(t)$, and $I_{cA}(t)$, $I_{cB}(t)$, $I_{cC}(t)$ are the input voltages and currents of the matrix converter, and $S_{ij}(t)$ is the switching function for $i$ is an element of {A,B,C} and $j$ is an element of {a, b, c}. Proper choice of $S$ will lead to a phase-reversal of the current so that the inductive load appears capacitive at the input to the MC [44, 45].

The controller uses the voltage measurement at the point of common coupling (PCC) and the instantaneous three-phase load currents decomposed into real and reactive components (based on SRF [35, 55, 56]). The voltage regulator part compares the measured PCC voltage value with the required reference to generate the required reactive current for voltage regulation which is added to the reactive load current component as in Fig. 2. The real component of the load current consists of a dc part that represents the fundamental component of the current and the ac part that represent the harmonics. The harmonic component is extracted and then transformed back to the ABC reference frame to be used as a reference current for the controller. More details on the controller are discussed in [44, 45].

### C. MPC based control strategy

The MPC-based controller has two functions as in Fig. 2. First, it predicts the future behavior of the system using the system model, second, it minimizes the error between the reference and the predicted signals in the next sampling period. This controller is simple to implement, and it has a fast-dynamic response. The discrete-time model estimates the current at the next sample ($k$+1) is given as [36]:

$$i_{oj}^{\sigma}(k+1) = \left(1 - \frac{R_{L_{MCj}} T_s}{L_{MCj}}\right) i_{oj}(k) + \frac{T_s}{L_{MCj}} v_{oj}(k) \quad (4)$$

where $\sigma$ is the switching configuration number, $\sigma \in \{1,..,27\}$, $v_{oj}(t)$ is the per-phase output voltage of the MC, $i_{oj}(t)$ is the per phase output current of the MC, $L_{MCj}$ and $R_{L_{MCj}}$ is the per-phase inductance and parasitic resistance of the output chokes and j is the output phases of the MC, $j \in \{A, B, C\}$.

The input reactive power and the input current of the converter can be written in orthogonal coordinates as:

$$\begin{aligned} i_{cn}^{\sigma}(k+1) = {} & A_{q(2,1)} V_{en}(k) + A_{q(2,2)} i_{cn}(k) \\ & + B_{q(2,1)} V_{Busn}(k) + B_{q(2,2)} i_e(k) \end{aligned} \quad (5)$$

The cost function $J$ is given as

$$\begin{aligned} J^{\sigma} = {} & \lambda_1 (|I_{cA}^{\sigma} - i_{cA}^*| + |I_{cB}^{\sigma} - i_{cB}^*| + |I_{cC}^{\sigma} - i_{cC}^*|) \\ & + \lambda_2 (|I_{oa}^{\sigma} - i_{oa}^*| + |I_{ob}^{\sigma} - i_{ob}^*| + |I_{oc}^{\sigma} - i_{oc}^*|) \end{aligned} \quad (6)$$

where $J$ is the cost function and $I_{cj}^{\sigma}$ is the predicted value of D-STATCOM input current and $I_{oj}^{\sigma}$ is the predicted value of MC output current with $j \in \{A, B, C\}$. Reference values $i_{cj}^*$ and $i_{oj}^*$ are the MC reference input and output currents respectively. The weight factors $\lambda_1$, $\lambda_2$ are adjusted to priorities the different parts of the cost function. In this paper, $\lambda_1$ is given a higher priority with the ratio $\lambda_1/\lambda_2 = 5$. Optimal tuning of these weight factor is still an open topic for research [57, 58]. In this paper, manual tuning of the weight factors is performed according to the guidelines from [58].

## IV. Power Systems Study and Results

### A. Description of distribution test system

With increasing penetration of distributed PV generation in the low-voltage (LV) distribution networks, bidirectional power flow becomes possible and can cause significant variation in voltage profile, as illustrated in Fig. 4. The LV distribution networks have special characteristics, such as dynamic loads, and high resistance/reactance (R/X) ratio [59]. The voltage deviation $\Delta V_g$ between bus-1 and 2 along the feeder, due to the current injection from bus-2, can be expressed as:

$$\Delta V_g = I_n Z_n \quad (7)$$

where $Z_n$ is the feeder impedance $(R_n + jX_n)$. The bus voltage deviation at the point of connection $V_g$ can be written as [59]:

$$\Delta V_g = \frac{R_n . P_g + X_n . Q_g}{|V_g|} + j \frac{X_n . P_g - R_n . Q_g}{|V_g|} \quad (8)$$

Using (8), the bus voltage can be approximated as in (9) [59]:

$$V_g \approx V_{g-1} + \frac{R_n . P_g + X_n . Q_g}{|V_g|} \quad (9)$$

where $P_g$ and $Q_g$ are the active and reactive power respectively at the point of connection. According to (8) and (9) the voltage drop between the buses depends on the active power, reactive power and the values of line impedance. It can be noticed that without PV, the power flows in one direction from the distribution transformer to the load, and this causes voltage reduction at bus-2 as in Fig. 4. On the other hand, voltage rise can occur due to the reverse power flow from the PV system to the grid. The amount of voltage rise depends on the associated reverse power flow and the line impedance between the bus and the closest voltage regulating devices. To keep the bus voltage profile within the acceptable levels, a utility owned compensator can be connected at bus-2 to provide the required compensation to control the voltage profile and allow more distributed PV integration in LV distribution networks.

### B. Parameters of the IEEE-34 bus system

To understand the system-wide impact of high PV penetration on distribution systems, the model of IEEE-34 bus test system is considered. The one-line diagram of the test system is shown in Fig. 3. The IEEE 34 bus test system is a 24.9 kV radial distribution network characterized by long lines and light loads. The circuit consists of a 2500 kVA, 69 kV/24.9 kV, Δ-Y substation transformer, two in-line three phase voltage regulators, an in-line 500 kVA, 24.9 kV/4.16 kV Δ-Y transformer at the start of the 832-890 lateral. The distribution system is also equipped with two three-phase fixed capacitor banks with a combined rating of 750 kVAR. A 300 kVAR three-phase shunt capacitor bank is connected to bus 844 while a larger 450 kVAR three-phase shunt capacitor bank is connected to bus 848.

The load center for the first in-line voltage regulator from

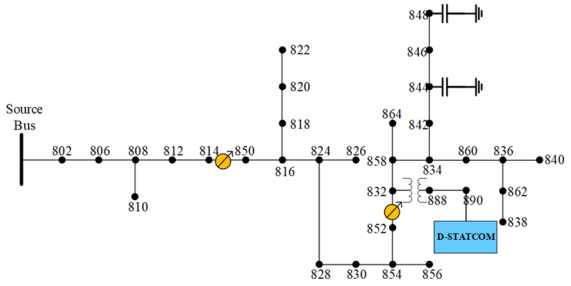


Fig. 3 One-line diagram of distribution system with high PV penetration. The proposed D-STATCOM is shown shunt connected at bus 890 to provide reactive power compensation.

the substation transformer (referred to as VR-1) is the bus 814R while the second voltage regulator (VR-2) controls the voltage of bus 852R. To control the load center voltage, both the voltage regulators make use of line drop compensation (LDC). The LDC acts a control circuit and models the voltage drop between the regulator and the load center to determine the tap position of the regulator. The LDC control circuit is shown in Fig. 5. The settings of the voltage regulators and the specifications of the LDC circuit are given in Table II. The settings for phase B and phase C are identical to phase A in both regulators. The defined setting for the bandwidth allows the load center voltage to be in the range of 121-123V for VR-1 and from 123-125 for VR-2.

The reason for a slightly higher voltage at the load center of VR-2 is to compensate for the large voltage drop in the 832-890 lateral. The time delay precludes the regulator to react to transient changes in the voltage or current. The regulators are equipped with a reversing switch which allows for a ±10 % regulation range in 32 steps. On a 120V base this translates to 0.75 V change per step.

### C. *OpenDSS simulation model*

In OpenDSS, the two three phase voltage regulators are modelled as six single phase two winding autotransformers with a regulator control unit for each autotransformer. Since the nominal feeder voltage is 24.9 kV, the rated voltage for the two windings of all single-phase autotransformers is 14.376 kV. The complete model of the distribution system consisting of all single-phase and three-phase overhead lines, feeder regulators, customer loads, capacitor banks, MV transformer, control circuits for the capacitor banks and voltage regulators and the substation transformer is developed in OpenDSS [60].

The aggregate peak active load of the IEEE 34 bus distribution test system as seen from the secondary of the substation transformer is 2.04 MW. Based on the nominal values of the loads, the individual bus loads were divided into four categories. The classification is given in Table III. A combination of different load models like constant power loads, constant impedance loads, constant current loads and voltage dependent loads to better represent the diversity of loads in MV/LV radial feeders were used. The use of such load models is consistent with the distribution test feeder specification developed by the working group of the IEEE distribution sub-committee. The dependency of the active and reactive loads on feeder voltages is modeled as

$$\frac{P_L(V)}{P_{L0}} = \left(\frac{V}{V_0}\right)^{\alpha} ; \frac{Q_L(V)}{Q_{L0}} = \left(\frac{V}{V_0}\right)^{\beta} \quad (10)$$

where the parameters $\alpha$ and $\beta$ define the exponential relationship of voltage $V$ with load active ($P_L$) and reactive ($Q_L$) power. $P_{L0}$ and $Q_{L0}$ are the nominal values of load active and reactive powers and $V_0$ is the base voltage.

### D. *Simulation considerations*

To study the effect of distributed generation, a proportional-distributed configuration of the grid-connected rooftop PV systems is chosen. This configuration is most typical of distribution systems with a significant percentage of residential loads. The capacity of the PV system is rated based on the active load at the bus. Each grid-connected PV system is equipped with an inverter with rating approximately 10% higher than the peak capacity of the PV system.

To account for the diversity in the roof top tilts and the

TABLE II
VOLTAGE REGULATOR SETTINGS

| Design Setting | VR-1(Phase A,B,C) | VR-2 (Phases A,B,C) |
|---|---|---|
| Voltage Level | 122V | 124V |
| Bandwidth | 2V | 2V |
| Time Delay | 15 seconds | 15 seconds |
| PT-Ratio | 120 | 120 |
| CT-Ratio | 100 | 100 |
| R | 2.7 V | 2.5 V |
| X | 1.6 V | 1.6 V |
| Connection | Wye-Wye | Wye-Wye |
| Location | Bus 814-814R | Bus 852-852R |

TABLE III
CLASSIFICATION OF LOADS ON IEEE 34 DISTRIBUTION SYSTEM

| Load Class | Nominal kW Range |
|---|---|
| Small Dwelling (Studio Apartment) | $P_L \leq 3\ kW$ |
| Large Dwelling (House with multiple bedrooms) | $3\ kW < P_L \leq 10\ kW$ |
| Small Scale Commercial | $10\ kW < P_L \leq 25\ kW$ |
| Medium Scale Commercial | $25\ kW < P_L \leq 100\ kW$ |
| Large Scale Commercial | $100\ kW < P_L \leq 500\ kW$ |

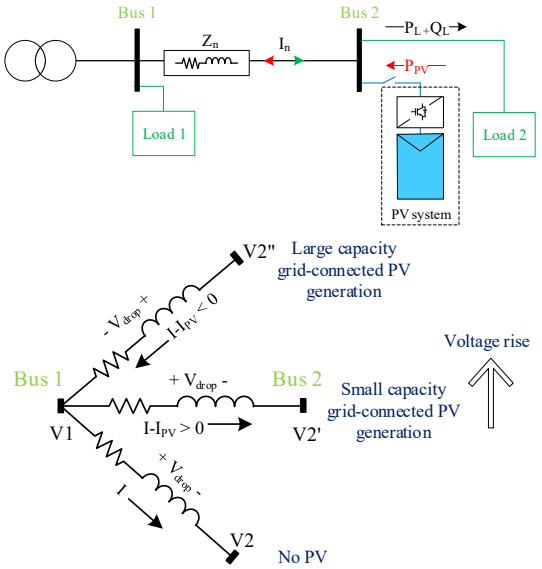


Fig. 4 Low voltage distribution network with high PV penetration scenarios. $V_2$ is the base-case bus voltage without PV. The voltage at bus-2 increases to $V_2'$ and $V_2''$ as more generation is added.

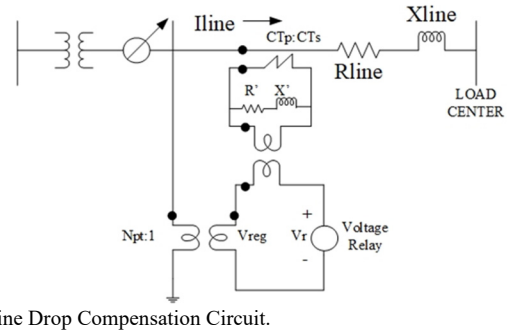


Fig. 5 Line Drop Compensation Circuit.

direction in which the roofs of the houses in a typical residential neighborhood are facing, the tilt angle and the azimuth angle of the roof top PV systems are sampled from a uniform distribution. The optimal azimuth angle of a grid-connected PV system in the northern hemisphere is 180° while the typical roof pitch in the U.S is 4/12-9/12. This corresponds to pitch angles in the range of 18.43°-36.87°. Hence, a truncated uniform density with a mean of 180° for the azimuth angle and a uniform density with a mean of 27° to model the tilt angle of the grid-connected rooftop PV systems was selected. The transposition model of [61] is used to incorporate the information of the tilt and azimuth angle with the annual solar irradiance data of 1 minute temporal resolution to estimate the real power output of the grid-connected PV systems.

To simulate the effect of distributed generation on the distribution system, a PV system is added to each load, with peak capacity chosen proportional to the peak active load at the bus. Each PV system is equipped with an inverter with rating approximately 10% higher than that of the PV panel to allow headroom to reactive power support. This is done to ensure a little headroom for the injection or absorption of reactive power. The PV penetration is given by

$$\%PV\ Penetration = \frac{\sum_{j=1}^{r} \psi_j^p}{\sum_{i=1}^{N} P_i^p} \times 100 \qquad (11)$$

where, $\psi_j^p$ is the rated peak active power of $j^{th}$ PV system, $P_i^p$ is the peak active load injection at $i^{th}$ bus, $r$ is the total number of PV systems deployed and $N$ is the total number of buses in the distribution system.

### *E. Results: Impact of high PV penetration*

With the legacy voltage control framework (substation LTC, in-line voltage regulators and Capacitor Banks) in operation, it is possible to control the slow variations in voltage due to load power injections. However, the stochastic nature of the PV generation results in highly variable voltages at the point of network connection. Such rapid excursions in bus voltages cannot be mitigated by legacy voltage control devices. The mechanical design of voltage regulators and switched capacitor banks renders them inadequate for regulating voltages at such shorter time scales of minutes and/or seconds. In fact, such highly fluctuating bus voltage profiles could stretch these devices to the limits of their operation and lead to premature failure of voltage regulators and switched capacitor banks. The results of the quasi-static time series (QSTS) simulations shown in this section demonstrate the impact of continuous reactive power support for voltage regulation on a three-phase distribution feeder with voltage regulators and switched capacitor banks.

To observe the impact of high PV penetration on distribution system voltage, the full three-phase model of IEEE-34 bus distribution test feeder is simulated in Open-DSS via a component object server (COMOS), that acts as a communication link between Open-DSS and MATLAB. Both steady state and (QSTS) simulations are performed to

TABLE IV
CUMULATIVE TAP OPERATIONS

| Device | Cumulative Tap Operations over a year | | |
|---|---|---|---|
| | PV ON, D-STATCOM OFF | PV ON, D-STATCOM ON | % Decrease in Tap Operation |
| VR-1A | 25,737 | 4,697 | 81.75% |
| VR-1B | 10,561 | 516 | 95% |
| VR-1C | 12,686 | 736 | 94.2% |
| VR-2A | 24,161 | 11,407 | 52.7% |
| VR-2B | 18,334 | 3,602 | 80.3% |
| VR-2C | 18,811 | 4,606 | 75.5% |

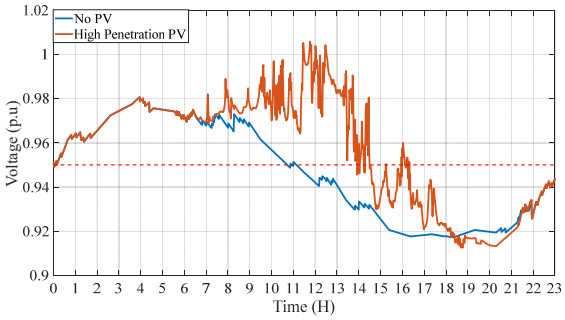


Fig. 6 Voltage profile of bus 890 with and without high PV penetration. Increased penetration of PV can lead to a rise in the bus voltage during times of high solar irradiation.

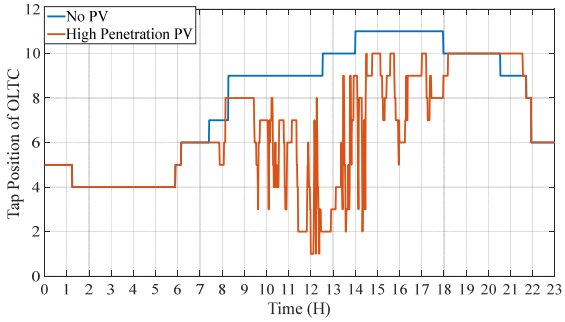


Fig. 7 OLTC tap position with and without high PV penetration. Increasing the penetration of PV requires more frequency changes in the tap positions, increasing mechanical wear.

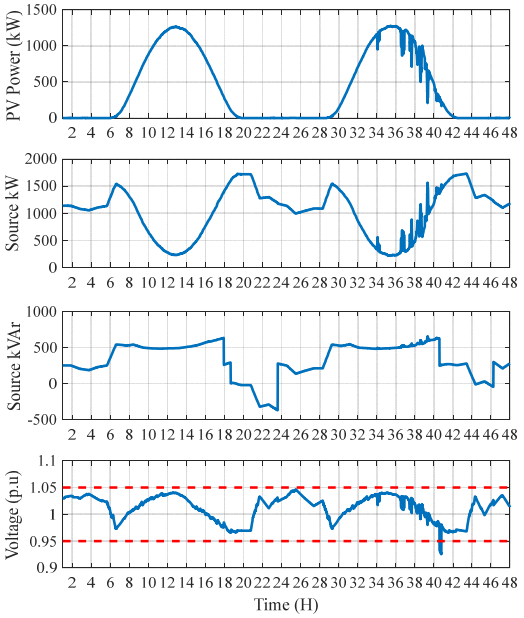


Fig. 8 Results from QSTS simulation showing power flow and bus voltage without D-STATCOM.

assess the impact of high capacitive PV generation (90% penetration level). The impact of a highly variable voltage on OLTC operation is presented in Fig. 6 and Fig. 7. The intermittent nonscheduled generation causes the OLTC to operate much more frequently to keep the voltage within the specified bandwidth.

The bus voltage profile as shown in Fig. 6 depicts a sustained increase in the voltage that lasts the entire duration the PV systems are generating power. When an OLTC or a switched capacitor encounters such a variable voltage on the secondary, it results in a significant increase in the operational frequency of such devices. The tap operation profile of an OLTC corresponding to the variable voltage of Fig. 6 is shown in Fig. 7. A high PV penetration disrupts the normal operation of OLTCs, which manifests in frequent changing of taps to correct for the fast voltage variations. However, it is clear that OLTCs are not able to regulate the voltage under conditions of high penetration of intermittent nonscheduled generation. Such an uncontrollable voltage profile could further lead to loss of load or at a worse result in a cascaded voltage collapse scenario. Since the penetration of PV systems has only increased over the last decade and based on the current trends, will continue to rise further. The utilities of the future need fast-acting voltage controllers that can provide reactive power compensation at sub-minute time scales to mitigate the undesirable effects on system voltage caused by intermittent nonscheduled generation.

The investment in reactive support with continuous control adjustment and a long service life is the most promising solution to combat the accelerated aging of mechanical assets in a distribution system. The proposed compensator is able to provide reactive power compensation as well as harmonic filtering at the source of the power quality problem, thereby eliminating the propagation of harmonics, voltage flicker and voltage fluctuations upstream toward the source i.e. distribution substation. To see the impact the proposed D-STATCOM would have on the tap-changing devices, a steady-state model of the D-STATCOM is developed in MATLAB and interfaced with OpenDSS via COM interface. The steady-state voltage regulation model of the proposed D-STATCOM is based on the reactive power mismatch equations. The model makes use of a proportional-integral (PI) controller to minimize the mismatch between the reference voltage and the measured bus voltage. The reactive power mismatch equations are:

$$\begin{bmatrix} Q_{cb} - V_{pcc} I \sin\left(\theta_{V_{pcc}} - \theta_I\right) \\ Q_{cb} + \left|V_{pcc}\right|^2 B - |V'| G \sin\delta + |V'| B \cos\delta \end{bmatrix} = 0 \quad (12)$$

where, $|V'| = |V_{pcc}||V_{conv}|$ and $\delta = \theta_{V_{pcc}} - \theta_{V_{conv}}$. In (12), $Q_{cb}$ is the reactive power exchanged between the converter and the bus where the converter is connected, $B$ and $G$ are the line susceptance and the conductance respectively, $V_{pcc}$ is the voltage at the point of common coupling and $V_{conv}$ is the converter voltage.

The interaction of the D-STATCOM with an OLTC is studied by connecting the two converters at Bus 890, which is on the secondary side of the voltage regulator-2 and at Bus 854, on the primary side of the voltage regulator-2. The operation of the two converters is coordinated with the OLTC by setting the reference voltage of the two converters equal to the voltage set point of the regulator. The voltage regulator

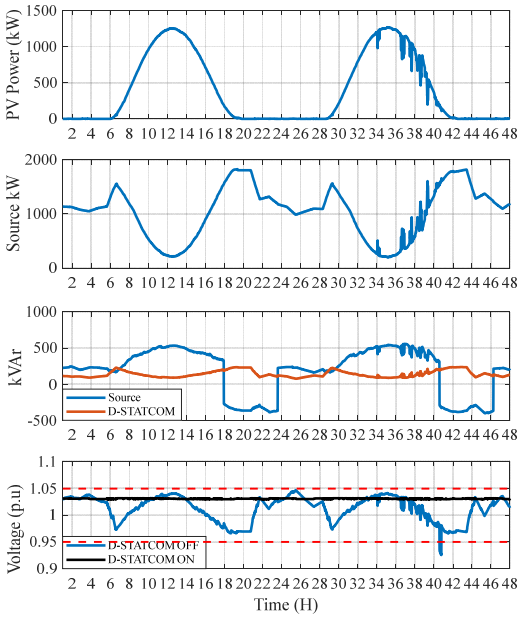


Fig. 9 Results from QSTS simulation showing power flow and bus voltage with D-STATCOM.

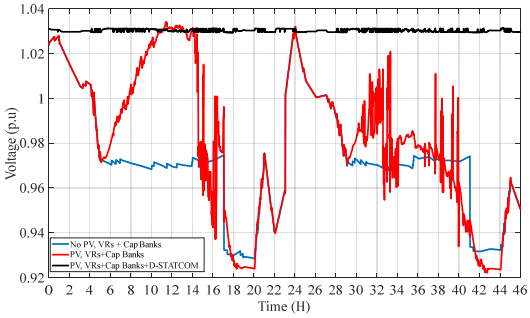


Fig. 10 Impact of D-STATCOM on voltage profile of bus 890 without and with high PV penetration.

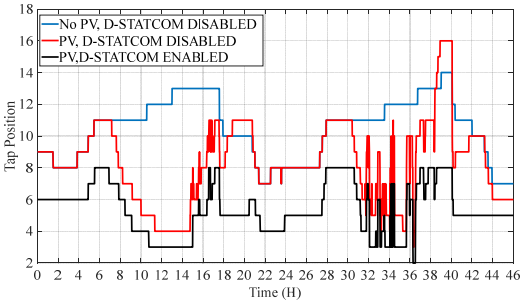


Fig. 11 Impact of D-STATCOM on OLTC operation without and with high PV penetration over a 48-hour period. With the D-STATCOM in operation, the black curve shows the tap position of the regulator as a function of time. The voltage regulator registers less operations with the D-STATCOM enabled than with D-STATCOM disabled. Over the course of a year, the D-STATCOM device has been shown to decrease voltage regulator tap operations by up to 95%.

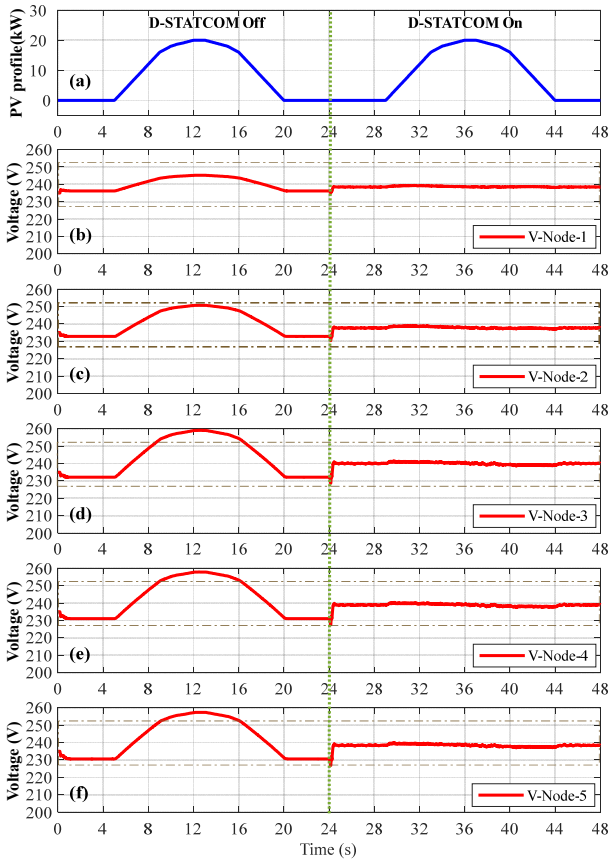


Fig. 12 Voltage profile at different buses on the distribution feeder. D-STATCOM is connected at bus-3. The final 24-hours is without the capacitorless D-STATCOM compensator. The second 24-hours assumes identical system operation but adds the capacitorless D-STATCOM device.

changes taps whenever the measured load center voltage is outside the specified bandwidth for a duration that exceeds the time delay of the regulator. Given a 90% PV penetration level, the IEEE-34 feeder is subjected to QSTS simulations and voltage of bus 890 and corresponding tap profile of regulator-2 is recorded.

Fig. 10 shows the voltage profile of Bus 890 under different feeder conditions for the planning period of 48 hours and the tap profile of voltage regulator-2 is shown in Fig. 11. Under high PV penetration and with D-STATCOM disabled, the bus voltage is highly variable and fluctuates rapidly. However, with the D-STATCOM enabled, the bus voltage is held nearly constant at 1.03 p.u. To ensure coordinated operation between the D-STATCOM and the voltage regulators, the voltage setting of the D-STATCOM is set equal to the voltage set-point of the nearest voltage regulator. With the D-STATCOM running in voltage regulation mode, OLTC registers less tap operations and this corresponds to a decreased level of operational stress on the regulator. A direct consequence of this is a decrease in the wear and tear of the regulator under conditions of high PV penetration. Furthermore, with the D-STATCOM turned on, the regulator consistently operates at lower tap positions and this is less likely to hit the maximum tap position. The results of the annual QSTS simulations with respect to the cumulative number of tap operations of all the six phases of the two voltage regulators are given in Table IV.

The continuously adjustable reactive power compensation capability of D-STATCOM could be further leveraged to provide a number of benefits such as minimize power losses, improve power factor and reduce harmonic losses. This could be achieved by optimizing the number, location and voltage set points of the converters. Since the reactive output of PV inverters is limited by the amount of real power generated, the D-STATCOM offers superior performance both in terms of capacity usage and control characteristics [29].

The injection/absorption of reactive power to regulate voltage alters the flow of power and changes the overall feeder demand as seen on the secondary of the substation transformer. The results are shown in Fig. 8 and Fig. 9 were obtained by running daily QSTS simulations on the IEEE-34 feeder with and without a D-STATCOM at bus 890 respectively. The voltage set point of the D-STATCOM is set equal to load center voltage at the secondary of the voltage regulator-2. This ensures coordinated operation of the OLTC and the D-STATCOM. The source power refers to the diversified demand (real and reactive) as seen on the secondary of the substation transformer.

## V. Power Electronics Results

### A. Simulation Results

MATLAB/Simulink platform is used to verify the effectiveness of the proposed capacitor-less D-STATCOM in providing the required dynamic compensation to the network. The system under study contains a three-phase source with series impedance to represent the upstream side of the distribution network, three-phase loads distributed through five buses, PV system with 20kW power. The proposed D-STATCOM device is connected at bus-3 as in Fig. 2. The impact of the D-STATCOM the distribution network shown in the figure bellow with high PV penetration is studied with the parameters shown in Table V.

As shown in Fig. 12 the voltage profile across the five buses is shown with and without D-STATCOM device being connected to bus-3. It can be seen that without D-STATCOM, the voltage profile is changing as the PV system power vary during the day. It can be observed that there is poor voltage regulation at the buses located at the end of the feeder, where the voltage violates the limits of 228 (0.95pu) and 252 (1.05pu).

When D-STATCOM device is connected to bus-3, it started to provide the required support to the network and the voltage profile is improved across the distribution feeder. The three-dimensional view of the voltage profile across the five buses is plotted in Fig. 13 and Fig. 14. In Fig. 13 the voltage profile without D-STATCOM is presented changing as the power flow change in the network, while, after adding the D-STATCOM device to bus-3, as in Fig. 14, it can be noted that capacitorless D-STATCOM device has managed to flatten then voltage profile in the bus where it is connected and in the other buses in the feeder.

### *B. Experimental results for the capacitorless D-STATCOM*

The proposed technology is validated experimentally using 7.5kVA prototype. System parameters listed in Table V is used in experimental tests. A reduced scale experimental prototype, as shown in Fig. 15, is developed to validate the capability and the effectiveness of the proposed capacitor-less D-STATCOM in providing the required support to low voltage distribution network. The setup consists of Upstream side (12kVA three-phase grid simulator NHR-9410), downstream side (Electronic load from Cinergia), D-STATCOM unit (7.5 kVA Matrix converter unit with three-phase inductors connected at its the output side), and control platform (dSPACE Scalexio) to control the matrix converter. The MC unit consists of nine IGBT modules SK60GM123, isolated gate drive circuits, current direction detection circuit, clamp circuit for overvoltage protection, voltage transducers LEM LV 25-p and current transducers LEM LP 55. The dSPACE control platform consists of a processing unit and LabBox™ with 4 FPGA modules each module has 5 ADC 14bit resolution, 10 digital I/O pins and 5 analogue output pins. The MPC strategy is implemented in dSPACE Scalexio processing unit, while the measurements and four-step commutation and protection are implemented in dSPACE LabBox™ unit. dSPACE ControlDesk™ software is used to supervise and control the experiment in real-time and view and store the experimental results and modify the desired control parameters during the experiment.

The impact of D-STATOCM device on downstream bus voltage profile is presented in Fig. 16, before connecting D-STATCOM to the bus, it can be noticed that upstream is providing the load with active power of 4.2 kW and reactive power of 3 kVAR, while the D-STATCOM reactive power is zero. Also, the active power change in the figure as the PV system inject 3,000 W of active power to downstream side. The voltage profile downstream is fluctuating and violating the limits set by ANSI standards which can negatively impact the consumers connected at this bus. After the proposed D-STATCOM device is shunt connected to downstream bus, it starts to inject a dynamic reactive power to the grid to enhance

TABLE V
SYSTEM PARAMETERS

| Parameter | Value |
|---|---|
| Voltage, VLL,rms | 415 V |
| Frequency | 50Hz |
| Output chokes inductance LMC | 24mH |
| Input filter resistance Rf, Lf | 1 Ω, 1mH |
| Input filter capacitor Cf/phase | 18 uF |
| Sampling time Ts | 40µs |
| Weight factor λ1 | 2 |
| Weight factor λ2 | 0.6 |
| Rs | 0.35 Ohm |
| Ls | 1 mH |

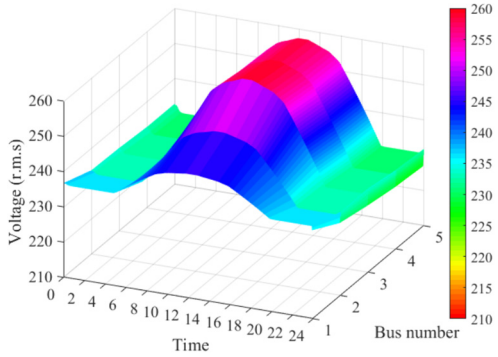


Fig. 13 Feeder voltage profile of the system in Fig. 2 without D-STATCOM device.

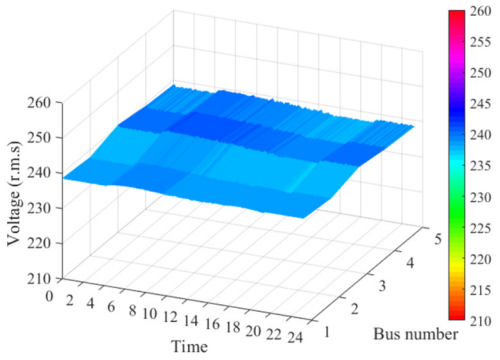


Fig. 14 Feeder voltage profile of the system in Fig. 2 with D-STATCOM connected at bus-3.

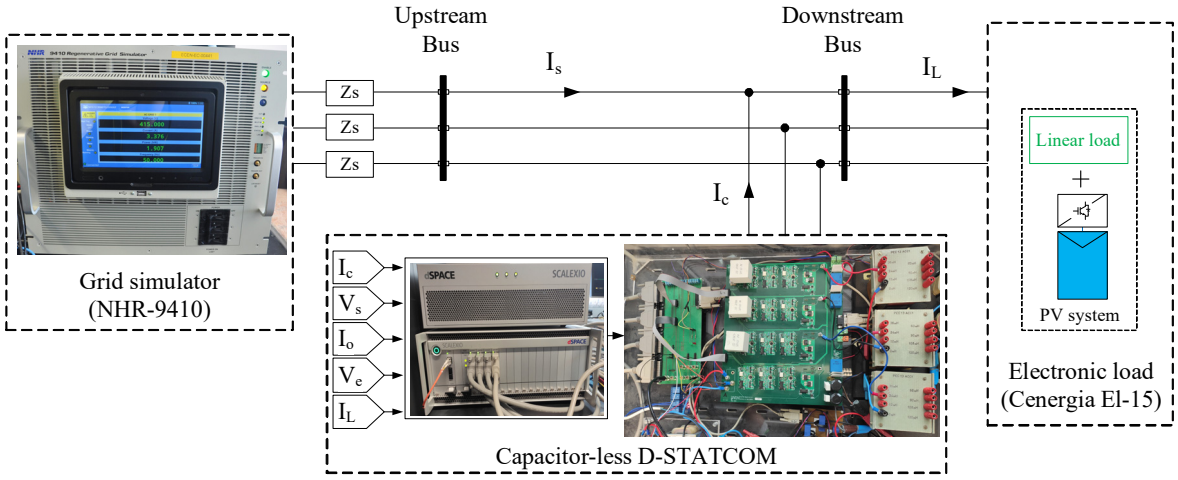


Fig. 15 Hardware setup of a 7.5kVA capacitor-less D-STATCOM system representing one bus in a radial destitution system. The upstream system is emulated by the grid simulator and the downstream loads are emulated by the electronic load.

the voltage profile. The capacitorless D-STACOM managed to flatten the voltage profile and it is tracking its reference 240V.

Upstream voltage ($V_s$) and current ($I_s$) without D-STATCOM support is plotted in Fig. 17, the source current lags the voltage and there is a phase shift between the voltage and the current. After the shunt-connected D-STATCOM device is enabled, it starts to provide the required support with source current now leading the voltage due to the reverse reactive power injection to the source to compensate for the voltage drop in the series impedance. D-STATCOM reference and measured current of phase A is shown in Fig. 18, the controller was able to track the reference current.

The upstream voltage distortion is still within the limits recommended by standards as shown in Fig. 19. Furthermore, the three-phase upstream current THD with D-STATCOM device is shown in Fig. 20. The current THD in Fig. 19 and Fig. 20 are within the limits specified by IEEE 519 [62, 63].

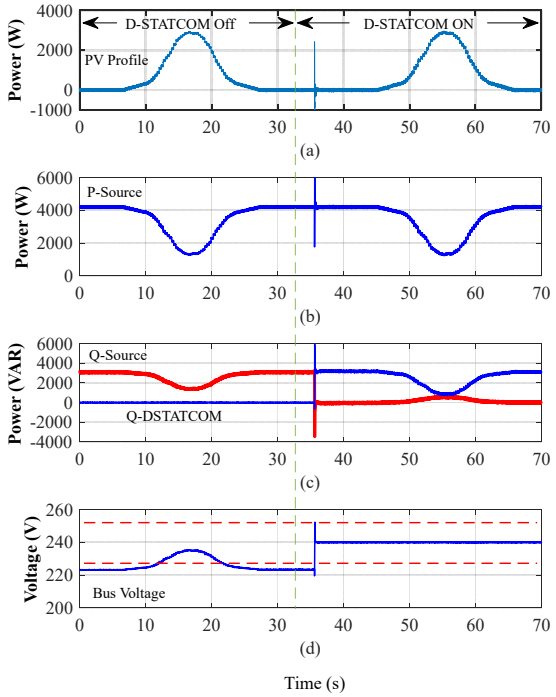


Fig. 16 Experimental results showing PV system profile, upstream power, and D-STATCOM power and voltage profile at downstream.

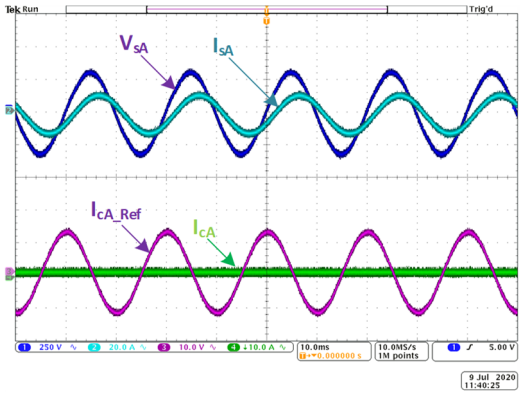


Fig. 17 Experimental results showing upstream voltage and current (VsA , IsA), and D-STATCOM reference and measured current (IcA_Ref , IcA) without D-STATCOM.

## VI. Discussions

Compared to other incumbent technologies, the capacitorless D-STATCOM is capable of dynamic reactive power compensation, dynamic voltage regulation, harmonic compensation, while being controlled by the network operator as was shown in Table I. A summary of the impact of the capacitorless D-STATCOM on a distribution network with high permeability is outlined and discussed in VI.CA. In

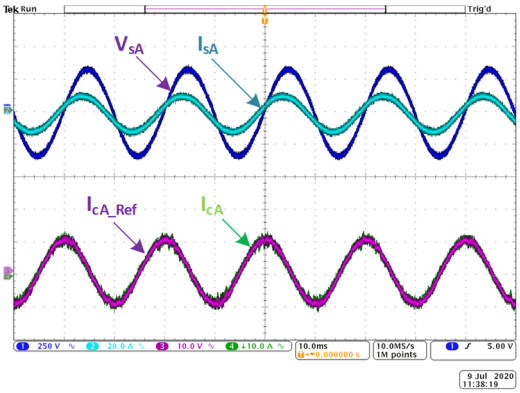


Fig. 18 Experimental results showing upstream voltage and current (VsA , IsA), and D-STATCOM reference and measured current (IcA_Ref , IcA) with D-STATCOM.

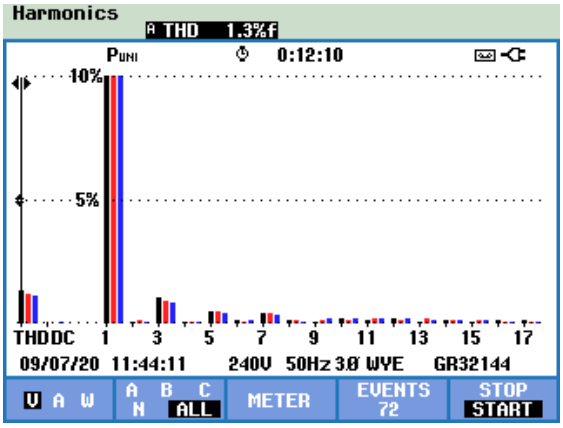


Fig. 19 Experimental results of upstream three phase spectra (Vs) with D-STATCOM device.

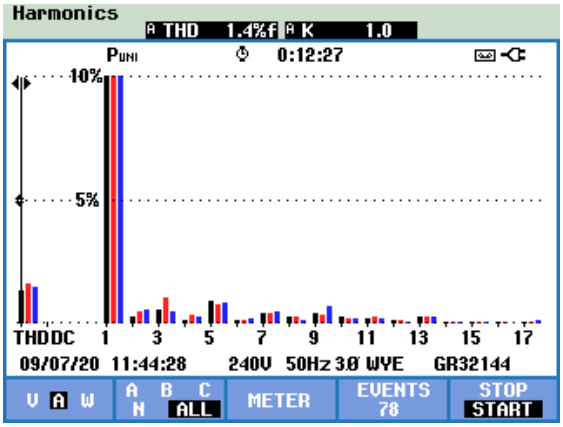


Fig. 20 Experimental results of upstream three phase current spectra (Is) with D-STATCOM device connected.

terms of impact, the capacitorless D-STATCOM has the same impact on the PV system as the incumbent voltage source converter-based (VSC) D-STATCOM technology. The only difference between the proposed capacitorless D-STATCOM and the incumbent D-STATCOM is the use of inductors instead of capacitors for energy storage. An impact and behavior comparison between the proposed capacitorless D-STATCOM and the incumbent D-STATCOM is discussed in VI.B with experimental results. A reliability comparison between the two technologies is further discussed in VI.C.

### *A. Impact of the capacitorless D-STATCOM on a distribution network with high PV permeability*

The main take aways from power system study presented in Section IV:

- Capacitorless D-STATCOM can perform VAR compensation and voltage regulation in the distribution network
- Dynamic harmonic compensation of the capacitorless D-STATCOM was shown to counteract PV variability in a distribution network with high PV permeability
- A distribution network with high PV penetration and a capacitorless D-STATCOM has shown less tap changes in network mechanical OLTCs. Thus, increasing the service life of already existing distribution network equipment.

### *B. Impact and behavior comparison between incumbent D-STATCOM and capacitorless D-STATCOM*

Experimental compensation effect comparisons between traditional VSC-based D-STATCOM and proposed capacitorless D-STATCOM. The phase A source voltage, source current, and source current harmonics at 200 V with non-linear connected are presented. Fig. 21(a) Results without STATCOM connected showing the impact of the non-linear load on the distribution network. Fig. 21(b) Results with VSC-based D-STATCOM illustrating improved harmonic compensation. Fig. 21(c) Results with the capacitorless D-STATCOM illustrating similar impact and behavior as the incumbent D-STATCOM technology.

### *C. Reliability comparison between incumbent D-STATCOM and capacitorless D-STATCOM*

Considering the main application of the capacitorless D-STATCOM is in hot weather environments, mission profile data based on Arizona, USA ambient temperatures is relevant to this analysis [64]. Keeping the reliability study succinct for this paper, failure rates are obtained from models presented in the military handbook MIL-HDBK-217F [65]. Since the handbook is old, the obtained component failure rates were adjusted to match with other recent work relying on Monte-Carlo analyses as in [66-69]. From [66], the equivalent static value for mean junction temperature was found to be $T'_{jm} = 31.55$ ℃ for the mission profile for the state of Arizona and is thus used in this study.

The circuit diagrams for the 7.5 kVA D-STATCOM experimental prototypes in section VI.B is shown in Fig. 22. In terms of characterizing the failure function, the converter-level reliability block diagrams of Fig. 23 (a) and (b) show the components connected in series, since a failure in any of the components, results in total failure of the converter. The converter-level reliability diagram of the VSC-D-STATCOM (Fig. 23(a)) is comprised of six switches with six body diodes and a capacitor bank of eight capacitors. The connection of dc link capacitors (series/parallel) is irrelevant in the reliability analysis, since one capacitor failure, tends to cascade to the other capacitors [70, 71]. Similarly, the converter-level reliability diagram for the capacitorless D-STATCOM (Fig. 23(b)) is comprised of eighteen switches with body diodes and three inductors.

Based on [65], the failure rates per year for the components of the D-STATCOM are $\lambda_D = 9.96 \times 10^{-6}$, $\lambda_Q = 1.89 \times$

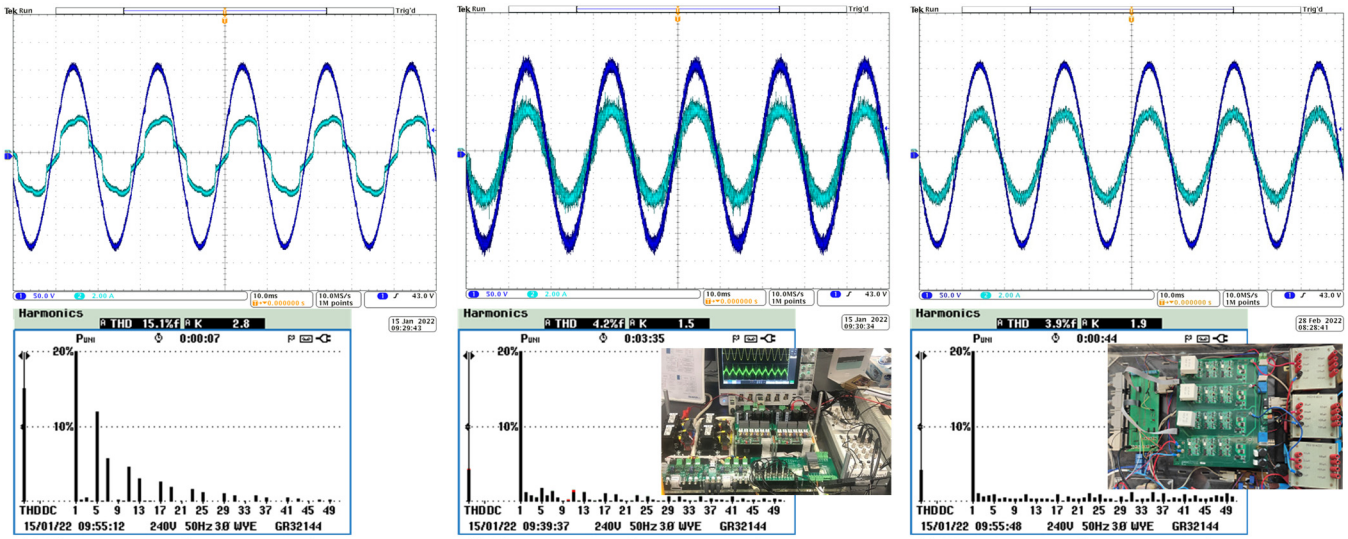


(a) Phase A source voltage, current and current harmonics without STATCOM connected.

(b) Phase A source voltage, current and current harmonics with VSC-based D-STATCOM connected.

(c) Phase A source voltage, current and current harmonics with capacitorless D-STATCOM connected.

Fig. 21 Experimental compensation effect comparisons between traditional VSC-based D-STATCOM and proposed capacitorless D-STATCOM. The phase A source voltage, source current, and source current harmonics at 200 V with non-linear connected are presented. (a) Results without STATCOM connected showing the impact of the non-linear load on the distribution network. (b) Results with VSC-based D-STATCOM illustrating improved harmonic compensation. (c) Results with the capacitorless D-STATCOM illustrating similar impact and behavior as the incumbent D-STATCOM technology.

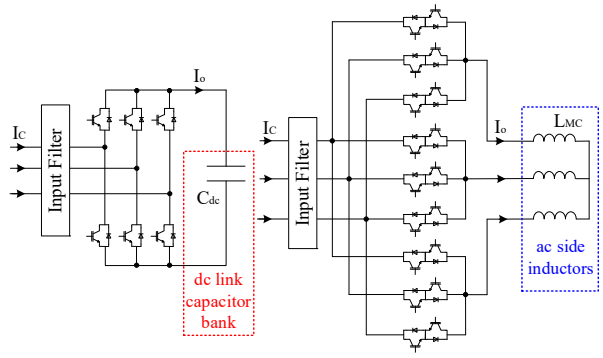


(a) VSC-based D-STATCOM (b) Capacitorless D-STATCOM

Fig. 22 Circuit diagrams used in the reliability studies (a) incumbent VSC-based D-STATCOM, and (b) proposed capacitorless D-STATCOM based on matrix converter (MC).

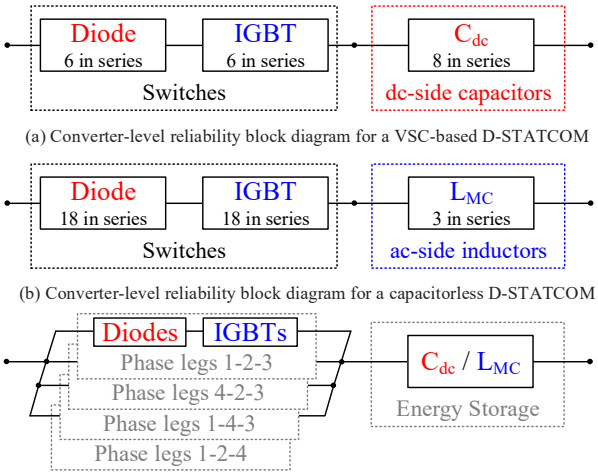


(a) Converter-level reliability block diagram for a VSC-based D-STATCOM

(b) Converter-level reliability block diagram for a capacitorless D-STATCOM

(c) Converter-level reliability of a fault-tolerant converter

Fig. 23 Converter-level reliability block diagram of the power switches, dc-side capacitors, and ac-side inductors for (a) incumbent VSC-based D-STATCOM, (b) proposed capacitorless D-STATCOM, (c) a fault-tolerant (four-legged) converter.

$10^{-3}$, $\lambda_L = 2.64 \times 10^{-4}$, and $\lambda_C = 7.84 \times 10^{-3}$ for the diode, IGBT, inductor, and capacitor respectively. The survival function of the exponential distribution can be used to model component failure function.

$$F_{com}(t) = 1 - e^{-\lambda t} \tag{13}$$

where $t$ is the time in years. The converter failure function $F_{conv}$ is calculated using

$$F_{conv}(t) = 1 - \prod \left(1 - F_{com}(t)\right) \tag{14}$$

Thus, the VSC-based D-STATCOM failure function is

$$F_{VSC}(t) = 1 - \left(1 - e^{-\lambda_D t}\right)^6 \left(1 - e^{-\lambda_Q t}\right)^6 \left(1 - e^{-\lambda_C t}\right)^8 \tag{15}$$

and the failure function of the capacitorless D-STATCOM can be written as

$$F_{MC}(t) = 1 - \left(1 - e^{-\lambda_D t}\right)^{18} \left(1 - e^{-\lambda_Q t}\right)^{18} \left(1 - e^{-\lambda_C t}\right)^3 \tag{16}$$

The converter-level unreliability function curves for both converters based on Arizona environmental conditions are shown in Fig. 24. Based on the data considered in this

TABLE VI
SUMMARY OF RELIABILITY ANALYSIS RESULTS

| Technology | VSC[1] | Capless[2] | FT VSC[3] | FT Capless[4] |
|---|---|---|---|---|
| 10-year reliability $R_{conv}(t = 10)$ | 48% | 71% | 53% | 99% |
| 25-year reliability $R_{conv}(t = 25)$ | 16% | 42% | 21% | 87% |
| Converter-level lifetime - $B_{10}$ | 1.4 years | 3.0 years | 1.7 years | 22.6 years |

[1] VSC-based D-STATCOM
[2] Capacitorless D-STATCOM
[3] Fault-tolerant VSC-based D-STATCOM
[4] Fault-tolerant Capacitorless D-STATCOM

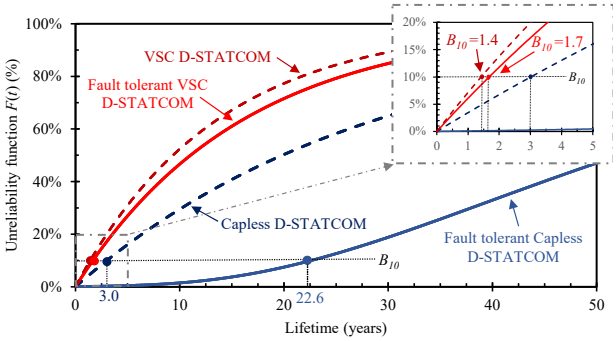


Fig. 24 Unreliability functions for the VSC-based D-STATCOM and the capacitorless D-STATCOM installed in Arizona environmental conditions.

analysis, Fig. 24 shows that the VSC-based D-STATCOM is more prone to failure than the capacitorless D-STATCOM. The reliability function $R_{conv}(t) = 1 - F_{conv}(t)$. Based on the components' statistics the reliability of the incumbent VSC-based D-STATCOM is $R_{VSC,10} = 48\%$, and the reliability of the proposed capacitorless D-STATCOM is $R_{MC,10} = 71\%$ over a 10-year period. Summary of the reliability analysis results are shown in TABLE VI. The system-level $B_{10}$ lifetimes, which correspond to the time by which the converter has 10% probability of failure, is shown in the same figure and summarized in Table VI. The $B_{10}$ lifetime of the proposed capacitorless D-STATCOM is shown to be 53% longer than the incumbent VSC-based D-STATCOM.

A three-year $B_{10}$ lifetime for the capacitorless D-STATCOM is still considered low, attributed mainly to the hot environment and to the number of switches of the matrix converter. Previous work has considered a fault-tolerant capacitorless D-STATCOM [72] and the experimental prototype in Fig. 15 is a four-legged matrix converter. The converter level reliability of a fault-tolerant converter is as shown in Fig. 23(c). In terms of the reliability of a fault-tolerant converter, the fourth phase leg provides a contingency path to any of the three phase legs and is thus represented as four parallel reliability paths. The reliability of the converter can be represented as

$$R_{conv} = \left[1 - \left(1 - e^{-(n_D \lambda_D + n_Q \lambda_Q)t}\right)^4\right] \cdot e^{-n_E \lambda_E t} \tag{17}$$

where $\lambda_E$ is the failure rate per year of the energy storage device ($\lambda_L$ for the inductor or $\lambda_C$ for the capacitor), $n_E$, $n_Q$

and $n_d$ are the number of energy storage devices, IGBTs and diodes respectively.

The unreliability functions of a fault-tolerant VSC-based D-STATCOM and a capacitorless D-STATCOM are plotted on Fig. 24. Considering a four-legged matrix converter in this study, increases $B_{10}$ lifetime of the capacitorless D-STATCOM to 22.6 years. A four-legged fault tolerant VSC-based D-STATCOM has a $B_{10}$ lifetime of 1.7 years. Thus, a fault-tolerant capacitorless D-STATCON has a 92.5% longer life than a fault-tolerant VSC-based D-STATCOM. Results of the reliability comparisons and the $B_{10}$ lifetimes are for a fault-tolerant capacitorless D-STATCOM compared to a fault tolerant VSC-based D-STATCOM are summarized in Table VI. From this study, data is shown to corroborate the initial motivation for this research that the dc link capacitors are the reliability bottleneck for the VSC-based D-STATCOM.

## CONCLUSION

This paper presented a detailed analysis and impact study of the capacitor-less D-STATCOM in high PV penetration distribution networks. The significance of this paper is that it studies the behavior of the power electronics converter and its interaction with the power systems, without assuming or neglecting details of either. In the power system study in this paper, a complete OpenDSS simulation of the IEEE 34 bus distribution test system was used to illustrate the impact of the capacitorless D-STATCOM during high PV penetration. In the power electronics study, in addition to mathematical formulation of the topology and controller, the electrical performance of the capacitorless D-STATCOM was demonstrated on a 7.5 kVA experimental prototype. The capacitorless D-STATCOM was shown to provide dynamic support to the distribution network to allow more PV penetration. Additionally, the capacitorless D-STATCOM could precisely control the voltage, be used to perform conservative voltage reduction to reduce losses, and improve the efficiency of the low voltage network.

## ACKNOWLEDGEMENT

This publication was made possible by NPRP grant # 9-204-2-103 from the Qatar National Research Fund (a member of Qatar Foundation). The statements made herein are solely the responsibility of the authors.

The authors acknowledge and thank Professor Pat Wheeler and Professor Lee Empringham from the power electronics and machine control group at the University of Nottingham, UK, for their collaboration on the matrix converter prototype design and fabrication.

## REFERENCES

[1] H. Anuta, P. Ralon, M. Taylor, and F. La Camera, "Renewable Power Generation Costs in 2019," *International Renewable Energy Agency, Abu Dhabi,* Jun 2020.

[2] IEA International Energy Agency. "PVPS 2019: Snapshot of Global PV Markets." www.iea-pvps.org (accessed.

[3] F. Shahnia and A. Ghosh, "Coupling of neighbouring low voltage residential distribution feeders for voltage profile improvement using power electronics converters," *IET Generation, Transmission & Distribution,* vol. 10, no. 2, pp. 535-547, Feb 2016, doi: 10.1049/iet-gtd.2015.1015.

[4] M. Thomson and D. G. Infield, "Impact of widespread photovoltaics generation on distribution systems," *IET Renewable Power Generation,* vol. 1, no. 1, pp. 33-40, Mar 2007, doi: 10.1049/iet-rpg:20060009.

[5] Y. Ueda, K. Kurokawa, T. Tanabe, K. Kitamura, and H. Sugihara, "Analysis Results of Output Power Loss Due to the Grid Voltage Rise in Grid-Connected Photovoltaic Power Generation Systems," *IEEE Transactions on Industrial Electronics,* vol. 55, no. 7, pp. 2744-2751, Jun 2008, doi: 10.1109/TIE.2008.924447.

[6] R. Tonkoski, D. Turcotte, and T. H. El-Fouly, "Impact of high PV penetration on voltage profiles in residential neighborhoods," *IEEE Transactions on Sustainable Energy,* vol. 3, no. 3, pp. 518-527, May 2012.

[7] J. de Oliveira Quevedo *et al.*, "Analysis and design of an electronic on-load tap changer distribution transformer for automatic voltage regulation," *IEEE Transactions on Industrial Electronics,* vol. 64, no. 1, pp. 883-894, Jul 2016.

[8] C. R. Sarimuthu, V. K. Ramachandaramurthy, K. R. Agileswari, and H. Mokhlis, "A review on voltage control methods using on-load tap changer transformers for networks with renewable energy sources," *Renewable and Sustainable Energy Reviews,* vol. 62, pp. 1154-1161, Sep 2016, doi: https://doi.org/10.1016/j.rser.2016.05.016.

[9] K. N. Bangash, M. E. A. Farrag, and A. H. Osman, "Smart Control of on Load Tap Changer deployed in Low Voltage Distribution Network," presented at the International Conference on Electric Power and Energy Conversion Systems (EPECS), 24-26 Nov, 2015.

[10] T. Aziz and N. Ketjoy, "Enhancing PV Penetration in LV Networks Using Reactive Power Control and On Load Tap Changer With Existing Transformers," *IEEE Access,* vol. 6, pp. 2683-2691, Dec 2018, doi: 10.1109/ACCESS.2017.2784840.

[11] C. K. Gan, C. Y. Lau, K. A. Baharin, and D. Pudjianto, "Impact of the photovoltaic system variability on transformer tap changer operations in distribution networks," *CIRED - Open Access Proceedings Journal,* vol. 2017, no. 1, pp. 1818-1821, 12-15 Jun 2017, doi: 10.1049/oap-cired.2017.0476.

[12] P. Kayal and C. K. Chanda, "Strategic approach for reinforcement of intermittent renewable energy sources and capacitor bank for sustainable electric power distribution system," *International Journal of Electrical Power & Energy Systems,* vol. 83, pp. 335-351, Dec 2016, doi: doi.org/10.1016/j.ijepes.2016.04.029.

[13] A. Ulinuha, M. A. S. Masoum, and S. M. Islam, "Optimal Scheduling of LTC and Shunt Capacitors in Large Distorted Distribution Systems Using Evolutionary-Based Algorithms," *IEEE Transactions on Power Delivery,* vol. 23, no. 1, pp. 434-441, Dec 2008, doi: 10.1109/TPWRD.2007.911166.

[14] D. Q. Hung and Y. Mishra, "Voltage fluctuation mitigation: fast allocation and daily local control of DSTATCOMs to increase solar energy harvest," *IET Renewable Power Generation,* vol. 13, no. 14, pp. 2558-2568, Aug 2019, doi: 10.1049/iet-rpg.2019.0223.

[15] Y. Ke, P. Huang, and T. Tseng, "Performance measurement of Static Var Compensators in distribution system," in *Proceedings of the SICE Annual Conference*, 18-21 Aug 2010, pp. 311-315.

[16] M. A. Talebi, A. Kazemi, A. Gholami, and M. Rajabi, "Optimal placement of Static VAR Compensators in distribution feeders for load balancing by genetic, algorithm," presented at the International Conference and Exhibition on Electricity Distribution (CIRED), 6-9 Jun, 2005.

[17] W. Zhaoyu, C. Hao, W. Jianhui, and M. Begovic, "Inverter-Less Hybrid Voltage/Var Control for Distribution Circuits With Photovoltaic Generators," *IEEE Transactions on Smart Grid,* vol. 5, no. 6, pp. 2718-2728, Sep 2014, doi: 10.1109/TSG.2014.2324569.

[18] M. Begovic, A. Peerzada, S. Mohan, R. Balog, and W. Rohouma, "Impact of Large Distributed Solar PV Generation on Distribution Voltage Control," in *Proceedings of the 52nd Hawaii International Conference on System Sciences*, Maui, Hawaii, 8-11 Jan 2019, pp. 3473-3482.

[19] T. S. Marco, "Design of a 1MVA Grid-Tied Photovoltaic Plant in Bugasong (Visayan Islands-Philippines)," Industrial Technologies Engineering, Engineering Projects Department, Polytechnic University of Valencia Valencia, Spain, 2018. [Online]. Available: http://hdl.handle.net/10251/106802

[20] A. Group. ABB Central Inverters PVS800 100 to 500kW [Online] Available: https://new.abb.com/docs/librariesprovider22/technical-documentation/pvs800-central-inverters-flyer.pdf?sfvrsn=2

[21] A. M. Howlader, S. Sadoyama, L. R. Roose, and S. Sepasi, "Distributed voltage regulation using Volt-Var controls of a smart PV inverter in a smart grid: An experimental study," *Renewable energy,* vol. 127, pp. 145-157, Nov 2018.

[22] P. Jahangiri and D. C. Aliprantis, "Distributed Volt/VAr Control by PV Inverters," *IEEE Transactions on Power Systems,* vol. 28, no. 3, pp. 3429-3439, Apr 2013, doi: 10.1109/TPWRS.2013.2256375.

[23] K. A. Alboaouh and S. Mohagheghi, "Impact of Rooftop Photovoltaics on the Distribution System," *Journal of Renewable Energy,* vol. 2020, pp. 1-23, Jan 2020.

[24] A. Safayet, P. Fajri, and I. Husain, "Reactive Power Management for Overvoltage Prevention at High PV Penetration in a Low-Voltage Distribution System," *IEEE Transactions on Industry Applications,* vol. 53, no. 6, pp. 5786-5794, Aug 2017, doi: 10.1109/TIA.2017.2741925.

[25] N. K. Roy, H. R. Pota, and M. J. Hossain, "Reactive power management of distribution networks with wind generation for improving voltage stability," *Renewable Energy,* vol. 58, pp. 85-94, Oct 2013, doi: https://doi.org/10.1016/j.renene.2013.02.030.

[26] A. R. Gupta and A. Kumar, "Impact of various load models on D-STATCOM allocation in DNO operated distribution network," *Procedia Computer Science,* vol. 125, pp. 862-870, 7-8 Dec 2018, doi: https://doi.org/10.1016/j.procs.2017.12.110.

[27] B. Singh and J. Solanki, "A Comparison of Control Algorithms for DSTATCOM," *IEEE Transactions on Industrial Electronics,* vol. 56, no. 7, pp. 2738-2745, Apr 2009, doi: 10.1109/TIE.2009.2021596.

[28] B. Singh, P. Jayaprakash, and D. P. Kothari, "A T-connected Transformer and Three-leg VSC Based DSTATCOM for Power Quality Improvement," *IEEE Transactions on Power Electronics,* vol. 23, no. 6, pp. 2710-2718, Dec 2008, doi: 10.1109/TPEL.2008.2004273.

[29] W. Rohouma, R. S. Balog, A. A. Peerzada, and M. M. Begovic, "D-STATCOM for harmonic mitigation in low voltage distribution network with high penetration of nonlinear loads," *Renewable Energy,* vol. 145, pp. 1449-1464, Jan 2020, doi: https://doi.org/10.1016/j.renene.2019.05.134.

[30] R. Yan, B. Marais, and T. K. Saha, "Impacts of residential photovoltaic power fluctuation on on-load tap changer operation and a solution using DSTATCOM," *ELSEVIER: Electric Power Systems Research,* vol. 111, pp. 185-193, Jun 2014, doi: 10.1016/j.epsr.2014.02.020.

[31] S. Srikanthan and M. K. Mishra, "DC Capacitor Voltage Equalization in Neutral Clamped Inverters for DSTATCOM Application," *IEEE Transactions on Industrial Electronics,* vol. 57, no. 8, pp. 2768-2775, May 2010, doi: 10.1109/TIE.2009.2022069.

[32] B. Singh, P. Jayaprakash, D. P. Kothari, A. Chandra, and K. A. Haddad, "Comprehensive Study of DSTATCOM Configurations," *IEEE Transactions on Industrial Informatics,* vol. 10, no. 2, pp. 854-870, Mar 2014, doi: 10.1109/TII.2014.2308437.

[33] C. Kumar and M. K. Mishra, "A Voltage-Controlled DSTATCOM for Power-Quality Improvement," *IEEE Transactions on Power Delivery,* vol. 29, no. 3, pp. 1499-1507, Apr 2014, doi: 10.1109/TPWRD.2014.2310234.

[34] D. Q. Hung, Y. Mishra, and G. Walker, "Reducing voltage fluctuations using DSTATCOMs and reactive power of PV inverters in a medium voltage distribution system," *The Journal of Engineering,* pp. 5274-5279, Aug 2019, doi: 10.1049/joe.2018.9279.

[35] F. Shahnia, S. Rajakaruna, and A. Ghosh, *Static Compensators (STATCOMs) in Power Systems*. Springer, 2015.

[36] C. Y. Reddy, V. Krishnakanth, R. Sanjay, V. N. V. Krishna, and R. Jayabarathi, "Laboratory implementation of Automatic Voltage Regulator," presented at the Biennial International Conference on Power and Energy Systems: Towards Sustainable Energy (PESTSE), 21-23 Jan, 2016.

[37] H. Keyhani, M. Johnson, and H. A. Toliyat, "A soft-switched highly reliable grid-tied inverter for PV applications," presented at the IEEE Applied Power Electronics Conference and Exposition (APEC), 16-20 Mar, 2014.

[38] S. Harb and R. S. Balog, "Reliability of Candidate Photovoltaic Module-Integrated-Inverter (PV-MII) Topologies-A Usage Model Approach," *IEEE Transactions on Power Electronics,* vol. 28, no. 6, pp. 3019-3027, Oct 2013, doi: 10.1109/TPEL.2012.2222447.

[39] C. Lachkar *et al.*, "Failure analysis of aluminum electrolytic capacitors based on electrical and physicochemical characterizations," presented at the International Reliability Physics Symposium (IRPS), 2-6 Apr, 2017.

[40] T. Orłowska-Kowalska, F. Blaabjerg, and J. Rodríguez, *Advanced and Intelligent Control in Power Electronics and Drives*. Springer, 2014.

[41] S. Yang, A. Bryant, P. Mawby, D. Xiang, L. Ran, and P. Tavner, "An industry-based survey of reliability in power electronic converters," *IEEE Transactions on Industry Applications,* vol. 47, no. 3, pp. 1441-1451, Mar 2011.

[42] L. F. Costa and M. Liserre, "Failure Analysis of the dc-dc Converter: A Comprehensive Survey of Faults and Solutions for Improving Reliability," *IEEE Power Electronics Magazine,* vol. 5, no. 4, pp. 42-51, Dec 2018, doi: 10.1109/MPEL.2018.2874345.

[43] M. B. Shadmand, S. Jain, and R. S. Balog, "Autotuning Technique for the Cost Function Weight Factors in Model Predictive Control for Power Electronic Interfaces," *IEEE J. of Emerg. and Sel. Topics in Power Electron.,* vol. 7, no. 2, pp. 1408-1420, Jun 2019, doi: 10.1109/JESTPE.2018.2849738.

[44] M. B. Shadmand, M. Mosa, R. S. Balog, and H. Abu-Rub, "Model Predictive Control of a Capacitorless Matrix Converter-Based STATCOM," *IEEE Journal of Emerging and Selected Topics in Power Electronics,* vol. 5, no. 2, pp. 796-808, 2017, doi: 10.1109/JESTPE.2016.2638883.

[45] W. Rohouma, R. S. Balog, A. A. Peerzada, and M. M. Begovic, "Capacitor-less D-STATCOM for reactive power compensation," presented at the IEEE 12th International Conference on Compatibility, Power Electronics and Power Engineering (CPE-POWERENG), 10-12 Apr, 2018.

[46] W. Rohouma, R. S. Balog, A. A. Peerzada, and M. M. Begovic, "Reactive Power Compensation of Time-Varying Load Using Capacitor-less D-STATCOM," presented at the International Conference on Power Electronics-ECCE Asia (ICPE ECCE Asia), Busan, South Korea, 27-30 May, 2019.

[47] W. Rohouma, R. S. Balog, A. A. Peerzada, and M. M. Begovic, "Development of a Capacitor-less D-STATCOM for Power Quality Improvement in Low Voltage Network," presented at the IEEE International Conference on Compatibility, Power Electronics and Power Engineering (CPE-POWERENG) 23-25 Apr, 2019.

[48] W. Rohouma, R. S. Balog, A. A. Peerzada, and M. M. Begovic, "D-STATCOM for a Distribution Network with Distributed PV Generation," presented at the International Conference on Photovoltaic Science and Technologies (PVCon), 4-6 Jul, 2018.

[49] W. Rohouma, M. Metry, R. S. Balog, A. A. Peerzada, and M. M. Begovic, "Adaptive Model Predictive Controller to Reduce Switching Losses for a Capacitor-Less D-STATCOM," *IEEE Open Journal of Power Electronics,* vol. 1, pp. 300-311, 2020, doi: 10.1109/OJPEL.2020.3015352.

[50] A. Anzalchi, A. Sundararajan, A. Moghadasi, and A. Sarwat, "High-Penetration Grid-Tied Photovoltaics: Analysis of Power Quality and Feeder Voltage Profile," *IEEE Industry Applications Magazine,* vol. 25, no. 5, pp. 83-94, Jul 2019, doi: 10.1109/MIAS.2019.2923104.

[51] M. Karimi, H. Mokhlis, K. Naidu, S. Uddin, and A. H. A. Bakar, "Photovoltaic penetration issues and impacts in distribution network – A review," *Renewable and Sustainable Energy Reviews,* vol. 53, pp. 594-605, Jan 2016, doi: https://doi.org/10.1016/j.rser.2015.08.042.

[52] F. Katiraei and J. R. Agüero, "Solar PV integration challenges," *IEEE Power and Energy Magazine,* vol. 9, no. 3, pp. 62-71, Apr 2011, doi: 10.1109/MPE.2011.940579.

[53] J. R. Agüero and S. J. Steffel, "Integration challenges of photovoltaic distributed generation on power distribution systems," presented at the IEEE Power and Energy Society General Meeting, 24-28 Jul, 2011.

[54] F. Blaabjerg, *Control of Power Electronic Converters and Systems*. Academic Press, 2018.

[55] S. Bhattacharya and D. Divan, "Synchronous frame based controller implementation for a hybrid series active filter system," presented at the IAS Annual Meeting, Industry Applications Conference, 8-12 Oct, 1995.

[56] B. Singh and V. Verma, "Selective Compensation of Power-Quality Problems Through Active Power Filter by Current Decomposition," *IEEE Transactions on Power Delivery,* vol. 23, no. 2, pp. 792-799, Mar 2008, doi: 10.1109/TPWRD.2007.911108.

[57] M. B. Shadmand, R. S. Balog, and H. Abu-Rub, "Auto-tuning the cost function weight factors in a model predictive controller for a matrix converter VAR compensator," presented at the IEEE Energy

Conversion Congress and Exposition (ECCE), Montreal, Canada, 20-24 Sep, 2015.
[58] P. Cortes *et al.*, "Guidelines for weighting factors design in Model Predictive Control of power converters and drives," presented at the IEEE International Conference on Industrial Technology, Feb, 2009.
[59] J. Hu, Z. Li, J. Zhu, and J. M. Guerrero, "Voltage stabilization: A critical step toward high photovoltaic penetration," *IEEE Industrial Electronics Magazine,* vol. 13, no. 2, pp. 17-30, Jun 2019.
[60] R. C. Dugan, "Reference guide: The open distribution system simulator (OpenDSS)." [Online]. Available: https://spinengenharia.com.br/wp-content/uploads/2019/01/OpenDSSManual.pdf
[61] C. A. Gueymard, "From global horizontal to global tilted irradiance: how accurate are solar energy engineering predictions in practice?," presented at the Solar 2008 Conference, San Diego, CA, 2008.
[62] I. W. Group, "519-2014 - IEEE Recommended Practice and Requirements for Harmonic Control in Electric Power Systems," *IEEE Std 519-2014 (Revision of IEEE Std 519-1992),* Standard pp. 1-29, Jun 2014, doi: 10.1109/IEEESTD.2014.6826459.
[63] "Voltage Disturbances, Standard EN 50160," in *Power Quality Application Guide*, ed. Wroclaw University of Technology: Copper Development Association, 2004.
[64] A. Andreas and S. Wilcox. *Observed Atmospheric and Solar Information System (OASIS) - SOLRMAP University of Arizona: 2018 Data*, http://dx.doi.org/10.5439/1052226.
[65] *Military Handbook: Reliability Prediction of Electronic Equipment*, Standard MIL-HDBK-217F Dec. 1991.
[66] A. Sangwongwanich, Y. Yang, D. Sera, and F. Blaabjerg, "Lifetime Evaluation of Grid-Connected PV Inverters Considering Panel Degradation Rates and Installation Sites," *IEEE Transactions on Power Electronics,* vol. 33, no. 2, pp. 1225-1236, 2018, doi: 10.1109/TPEL.2017.2678169.
[67] K. Ma, H. Wang, and F. Blaabjerg, "New Approaches to Reliability Assessment: Using physics-of-failure for prediction and design in power electronics systems," *IEEE Power Electronics Magazine,* vol. 3, no. 4, pp. 28-41, 2016, doi: 10.1109/MPEL.2016.2615277.
[68] D. Zhou and F. Blaabjerg, "Converter-Level Reliability of Wind Turbine With Low Sample Rate Mission Profile," *IEEE Transactions on Industry Applications,* vol. 56, no. 3, pp. 2938-2944, 2020, doi: 10.1109/TIA.2020.2977301.
[69] H. Wang *et al.*, "Transitioning to Physics-of-Failure as a Reliability Driver in Power Electronics," *IEEE Journal of Emerging and Selected Topics in Power Electronics,* vol. 2, no. 1, pp. 97-114, 2014, doi: 10.1109/JESTPE.2013.2290282.
[70] D. Zhou, Y. Song, Y. Liu, and F. Blaabjerg, "Mission Profile Based Reliability Evaluation of Capacitor Banks in Wind Power Converters," *IEEE Transactions on Power Electronics,* vol. 34, no. 5, pp. 4665-4677, 2019, doi: 10.1109/TPEL.2018.2865710.
[71] J. M. Lenz, A. F. Cupertino, H. A. Pereira, D. Zhou, H. Wang, and J. R. Pinheiro, "Benchmarking of capacitor power loss calculation methods for wear-out failure prediction in PV inverters," *Microelectronics Reliability,* vol. 100-101, p. 113491, 2019/09/01/ 2019, doi: https://doi.org/10.1016/j.microrel.2019.113491.
[72] W. Rohouma, R. S. Balog, A. A. Peerzada, and M. M. Begovic, "Fault-Tolerant D-STATCOM based Matrix Converter," in *2019 2nd International Conference on Smart Grid and Renewable Energy (SGRE)*, 19-21 Nov. 2019 2019, pp. 1-6, doi: 10.1109/SGRE46976.2019.9020698.